Unsupervised *Toxoplasma gondii* Recognition by Fuzzy Cycle Generative Adversarial Network

Sen Li[1] , **Aijia Li**[1] , **Diego Alejandro Molina Lara**[2] , **Jorge Enrique Gómez Marín**[2] , **Yang Zhang**[1*]

zhangyang07@hit.edu.cn

Abstract

$Toxoplasma\ gondii$, one of the world's most common parasites, can infect all types of warm-blooded animals, including one-third of the world's human population. Most of current routine methods of diagnosis are costly, time-consuming, and labor-intensive. The parasite can be directly observed under the microscope in tissue or spinal fluid samples, and this form of testing is cheap, but used less frequently because of the difficulty in operation, and needs well trained professionals. Nevertheless, observation of parasites in patient or animal specimens under the microscope is still performed by a large number of laboratories. The identification of Toxoplasma parasite with cost-effectiveness solution is still a health challenge in developing countries. Here, we propose an Artificial Intelligence (AI)-powered microscopic image analysis method for $Toxoplasma\ gondii$. The method uses Fuzzy Cycle Generative Adversarial Network (FCGAN) with transfer learning, by applying knowledge gained by the parasitologists that $Toxoplasma\ gondii$ is in banana or crescent shaped form. Our approach aims to build connection between micro and macro associated objects by embedding fuzzy C-means cluster algorithm into Cycle GAN. We show the high accuracy and effectiveness of our approach in the newly collected 28,130 unlabeled microscopic images from Toxoplasma infection samples.

1 Introduction

$Toxoplasma\ gondii$ ($T.gondii$) is an ubiquitous, single cell protozoan parasite that can infect all warm-blooded animals as well as one-third of human population worldwide[Khan and Grigg, 2017]. Most infections in humans are life-long and several studies have suggested that such infections may contribute to severe neurological and psychiatric symptoms. That makes diseases caused by $T.gondii$ is one of the biggest healthcare problem globally. Diagnosis of $T.gondii$ is typically by testing blood or other body fluids for antibodies or the parasite's DNA [Burrells *et al.*, 2018]. The parasite can be directly observed under the microscope in tissue or spinal fluid samples, and this form of testing is used less frequently because of the difficulty in operation, and needs well trained professionals. Nevertheless, observation of parasites in patient or animal specimens under the microscope is still performed by a large number of laboratories.

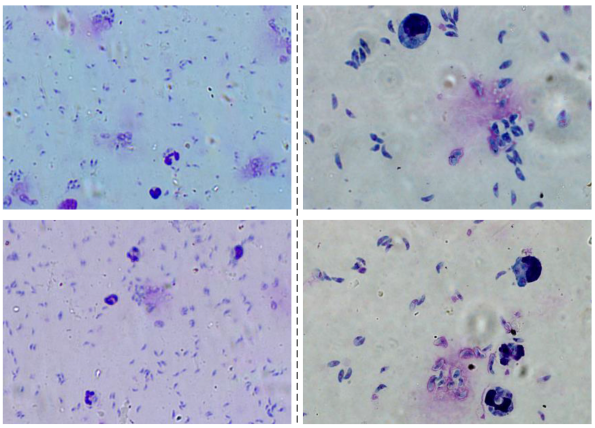

(a) Different FoV in 400X microscope (b) Different FoV in 1000X microscope

Figure 1: Typical variations of color, illumination, background in different fields of view and microscope magnification. (a) Images from different slides captured by a microscope with 400X magnification; (b) Images from different slides captured by a microscope with 1000X magnification.

However, the detection and quantification of $T.gondii$ under microscope is highly time-consuming, labor-intensive and needs well trained professionals to recognize. Moreover, the intensity of illumination, image brightness, contrast level and background of staining, have large variations in different Filed of View (FoV). In addition, $T.gondii$ is found both inside and outside of nucleated cells with separated and aggregated form, which makes $T.gondii$ recognition task more challenging (Figure 1).

Recently, deep learning technology has significantly improved the efficiency and accuracy in macroscopic computer vision task, thereby attracting considerable attention in microscopic image analysis [Christiansen *et al.*, 2018; Loddo *et al.*, 2018; Gecer *et al.*, 2018; Xing *et al.*, 2018]. Sivaramakrishnan Rajaraman et al. [Rajaraman *et al.*, 2018] evaluated

*Contact Author

the performance of pre-trained CNN as feature extractor in the classification of parasites and host cells, which improved the infection disease screening. Mehanian et al.[Mehanian *et al.*, 2018] developed a computer vision system with deep learning to identify malaria parasites under microscope for field-prepared thick blood films. Among existing deep learning methods on parasite analysis, most of them are under supervised learning framework, which requires many well-trained professionals to label a large amount of image dataset for training. Besides, labeling, annotating, and sorting information is time consuming, costly, and labor-intensive with well-trained professionals needed. This severely limits their scalability in practical applications.

Moreover, current existing parasite recognition models are limited on malaria only, and there is no solution available for toxoplasma. Here, we first propose an unsupervised learning method for $T.gondii$ recognition. To improve learning efficiency in the task, we employ transfer learning strategy by leveraging knowledge from the parasitologists that $T.gondii$ is in crescent shaped form, which is similar to banana. Even more, the shape of aggregated parasites resembles the images of a bunch of bananas, where host cells are significantly different. It is assumed that microscopic object has an inherent connection with macroscopic world. Based on this assumption, we design a Micro-Macro objects associated pulling (M2OAP) strategy and propose a Fuzzy Cycle Generative Adversarial Network (FCGAN) for unsupervised $T.gondii$ recognition.

The contributions of this work are summarized below:

• We are the first to study $T.gondii$ recognition task using deep learning algorithm. Our designed method uses an Micro-Macro Associated Objects Pulling (M2AOP) strategy for unsupervised microscopic object recognition. Inspired by the parasite experts, a pair of encoder and decoder were build to pull the $T.gondii$ close to a common object (like banana) in macroscopic world and pull the host cell away with a large distance. This strategy can exploit more discriminative information using a third associated object to asymmetrically pull $T.gondii$ and host cell samples.

• We propose a Fuzzy Cycle Generative Adversarial Network according to M2OAP strategy, which embed fuzzy C-means cluster algorithm into Cycle GAN. In detail, FCGAN can learn degrees of membership belonging to each cluster (class) point, and utilize degrees as the translated coefficient to replace the microscopic and macroscopic domain labels in Cycle GAN when the microscopic images are inductive transferred into macroscopic world.

• We introduce two $T.gondii$ image datasets which consist totally 13,138 microscopic images with magnification of 400X and 14,992 microscopic images with magnification of 1000X. A number of experiments are conducted demonstrating effectiveness of our fuzzy Cycle GAN method with recognition accuracy of *98.6%*, F1-score of *0.494*, recall of *0.986*, precision of *0.991*, and AUC of *0.951* in ROC curves under 400X microscopic images, and recognition accuracy of *88.3%*, F1-score of *0.434*, recall of *0.818*, precision of *0.925*, and AUC of *0.969* in ROC curves under 1000X microscopic images,

2 Fuzzy Cycle Generative Adversarial Network

Our proposed method is empowered by a Micro-Macro associated objects pulling strategy for unsupervised microscopic parasite recognition. As illustrated in Figure 2, we utilize Fuzzy Cycle Generative Adversarial Network, where cycle-consistency and associated objects pulling loss are optimized along with a fuzzy C-means algorithm.

2.1 Micro-Macro Associated Object Pulling Strategy

A set of unlabeled microscopic images is classified as target domain $\mathcal{T}$ including $T.gondii$ and host cells, another set of its associated macro object images is used as source domain $\mathcal{S}$, such as bananas. It is expected that source data shares the same cluster point with target $T.gondii$ images, and host cell images belong to another cluster point. Then we calculate the degree of membership of each cluster point for each sample in $\mathcal{T}$. Furthermore, an image translator is used to pull the target $T.gondii$ images closer to source banana images and the host cell images away from banana, which is achieved by replacing the domain label with the degrees of membership of each cluster point. Through the whole process, labeling of $\mathcal{T}$ is not required and necessary. We integrate Cycle GAN to the image translator combined with a fuzzy C-means algorithm to enhance its selectivity.

2.2 Why is Cycle GAN

For a set of unannotated target domain $\mathcal{T}$ and its desired associated source domain $\mathcal{S}$, Cycle GAN can learns two mappings without any supervision, $G : \mathcal{S} \rightarrow \mathcal{T}$ and $F : \mathcal{T} \rightarrow \mathcal{S}$ with two generators G and F, at the same time. To by pass the infeasibility of pixel-wise reconstruction with paired data, i.e. $G(\mathcal{S}) \approx \mathcal{T}$ or $F(\mathcal{T}) \approx \mathcal{S}$, Cycle GAN introduces an effective cycle-consistency loss for $F(G(\mathcal{S})) \approx \mathcal{S}$ and $G(F(\mathcal{T})) \approx \mathcal{T}$. The idea is that the generated target domain data is able to return back to the exact data in the source domain where it generated from. To guarantee the fidelity of fake data $G(\mathcal{S})$ and $F(\mathcal{T})$, Cycle GAN uses two discriminators $D_{\mathcal{S}}$ and $D_{\mathcal{T}}$ to distinguish real or synthetic data and thereby encourage generators to synthesize realistic data.

To solve the task of learning generators with paired images from two domains, $\mathcal{S}$ and $\mathcal{T}$, we adopt the idea of the original cycle-consistency loss [Zhu *et al.*, 2017] for generators G and F forcing the reconstructed synthetic sample $F(G(x_{\mathcal{S}}))$ and $G(F(x_{\mathcal{T}}))$ to be identical to their inputs $x_{\mathcal{S}}$ and $x_{\mathcal{T}}$.

$$\begin{aligned} L_{cyc}(G,F) = & E_{x_{\mathcal{S}} \sim P_{data}(\mathcal{S})}[\|F(G(x_{\mathcal{S}})) - x_{\mathcal{S}}\|_1] \\ & + E_{x_{\mathcal{T}} \sim P_{data}(\mathcal{T})}[\|G(F(x_{\mathcal{T}})) - x_{\mathcal{T}}\|_1] \end{aligned} \tag{1}$$

where $x_{\mathcal{S}}$ is images from source domain $\mathcal{S}$ and $x_{\mathcal{T}}$ is from target domain $\mathcal{T}$. L_{cyc} uses the L1 loss, which shows better visual results than the L2 loss.

2.3 Challenges in M2AOP Strategy

Lacking supervision with a direct reconstruction error between $G(\mathcal{S})$ and $\mathcal{T}$ or $F(\mathcal{T})$ and $\mathcal{S}$ brings some uncertainties and difficulties towards to the desired strengthened output of $T.gondii$ and weakened output of host cells. The conventional Cycle GAN cannot evaluate the importance of each

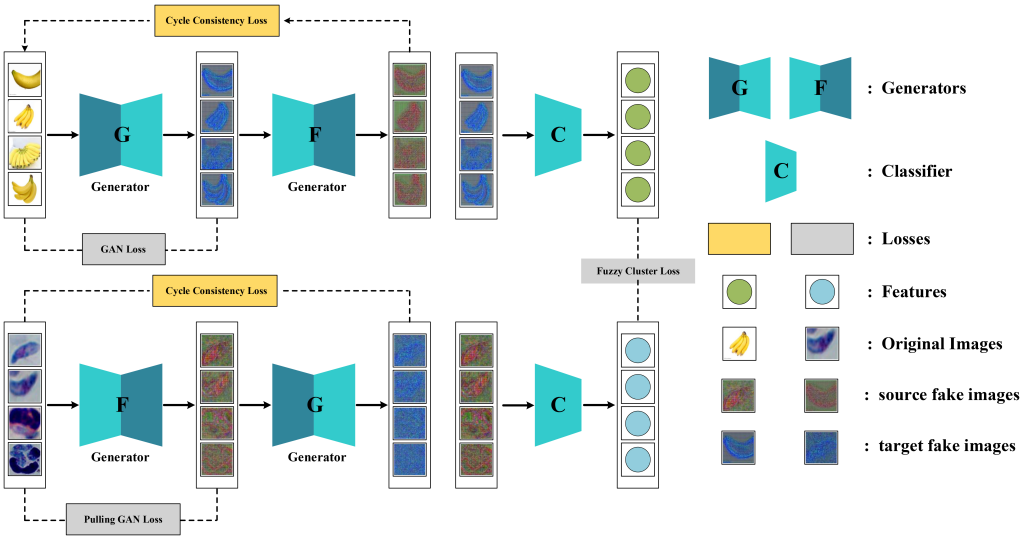

Figure 2: Illustration of our Fuzzy Cycle GAN. Losses are shown in dashed rectangles. After training with source and target data alternatively, the generators G and F are used to pull $T.gondii$ into source domain and try to remain host cells stay in target domain refer to their shape and texture information. Note that discriminators $D_{\mathcal{S}}$ and $D_{\mathcal{T}}$ are not drawn.

sample and it will transform all images in $\mathcal{T}$ domain without any selective ability. That makes our task even more challenging.

Such problem cannot exploit the discriminative information from the associated object in $\mathcal{S}$ and cannot select effective target samples from $\mathcal{T}$ to pull in an unsupervised manner. Our goal is to pull target $T.gondii$ images more closer to banana images in $\mathcal{S}$ and make the other host cell images remain a large distance between source banana images. So, we design the Fuzzy Cycle GAN approach and illustrate FCGAN as source-target image translated consistency, fuzzy pulling cluster generator and discriminator, optimization of FCGAN.

2.4 Fuzzy C-means Embedded in Cycle GAN

Aiming to obtain selective ability of Cycle GAN in unsupervised framework on $T.gondii$ recognition, we consider using cluster algorithm to solve this problem. Specifically, fuzzy clustering algorithm resolves this dilemma by introducing a degree of membership for each data point belonging to arbitrary number of clusters [Klir and Yuan, 1995].

We embed the degree of membership into Cycle GAN which denotes the degree of each sample belonging to $T.gondii$ cluster point and host cell point where we assume that $T.gondii$ shares a same cluster point with banana images in $\mathcal{S}$. We assume that which cluster closer to source banana point is the $T.gondii$ cluster point, and the other point is host cell images. Then, we develop the generator loss especially for discriminators embedded with degrees of membership belonging to cluster point of source domain $\mathcal{S}$ and embedded the degrees to host cell point in target domain $\mathcal{T}$ into adversarial loss, which could make embedded Cycle GAN strengthen the generative ability for samples belonging to $\mathcal{S}$ group by higher degree, weaken the generative ability for samples belonging to host cell group by lower degree, so as to pulling a relative larger distance for real $T.gondii$ than host cell images. The consequence of embedded Cycle GAN is making two cluster points of $T.gondii$ and host cell have a larger distance than the translation by fuzzy Cycle GAN before.

For this idea, we introduce the Fuzzy C-Means (FCM) algorithm [Bezdek, 1973]. To lean representative feature, we design a feature extractor C improved from VGG network [Simonyan and Zisserman, 2014]. For images $\{x_1, \cdots, x_k, \cdots, x_N\}$ in target domain $\mathcal{T}$ in parameter initialization (their translated fake source images are $\{F(x_1), \cdots, F(x_k), \cdots, F(x_N)\}$), we can get their feature space after translation of $\{C(F(x_1)), \cdots, C(F(x_k)), \cdots, C(F(x_N))\}$ through the feature extractor C. We want to partition these features into P clusters $\{v_1, \cdots, v_i, \cdots, v_P\}$ with minimization of the following objective function:

$$L_{fuzzy} = \sum_{i=1}^{P} \sum_{k=1}^{N} u_{ik}^{m} \|C(F(x_k)) - v_i\|^2 \tag{2}$$

where, x_k is the kth image in $\mathcal{T}$, v_i is d-dimensional center of the i-th cluster, u_{ik} denotes the degree of membership of feature $C(F(x_k))$ to cluster v_i, N is the total number of features in each domain, $\|C(F(x_k)) - v_i\|$ is any norm expressing the similarity between the measured feature $C(F(x_k))$ and the cluster center v_i. m denotes a weighting exponent parameter ($m > 1$) on each fuzzy membership value, and it determines the amount of fuzziness of the resulting classification according to:

$$U \left\{ u_{ik} \in [0,1]; \sum_{i=1}^{P} u_{ik} = 1, \forall k; 0 < \sum_{k=1}^{N} u_{ik} < N, \forall i \right\} \tag{3}$$

The first main step of this iterative algorithm is to update the membership function to determine in which cluster the feature belongs according to Eq.4:

$$u_{ik} = \frac{1}{\sum_{j=1}^{C} \left(\frac{\|v_i - C(F(x_k))\|}{\|v_j - C(F(x_k))\|} \right)^{\frac{2}{(m-1)}}} \tag{4}$$

Algorithm 1 Fuzzy Cycle Generative Adversarial Network

1:**Input:** Training set $X_{\mathcal{S}}$, $X_{\mathcal{T}}$; a weighting exponent parameter m, the clusters number P, and fuzzy update interval $loop$
2:**Initialization:** Initialize weight parameters in our network and degrees matrix $U^{(0)}$ and its correlated cluster center vector $V^{(0)}$
for $iterations = 0$ to M, $t = 0$ **do**
  Sample a mini-batch $x_{\mathcal{S}} \in \mathcal{S}, x_{\mathcal{T}} \in \mathcal{T}$
  Update G, F, $D_{\mathcal{S}}$, $D_{\mathcal{T}}$ by descending the gradient according L_{cyc}, L_{fuzzy}, L_F, L_G, $L_{D_{\mathcal{S}}}$, $L_{D_{\mathcal{T}}}$, $L_{pulling}$ of Eq.1, 2,6,7,8 using back-propagation algorithm.
  if $iterations\%loop == 0$ do
    $t = t + 1$
    Update the membership of U^{t+1} function using Eq.4.
    Update the cluster centers of V^{t+1} function using Eq.5.
    Update the membership of L_{fuzzy}^{t+1} function using Eq.2.
end for

The second main step concerns the updated centroids based on the new membership matrix according to Eq.(5):

$$v_i(x) = \frac{\sum_{k=1}^{N} (u_{ik})^m C(F(x_k))}{\sum_{k=1}^{N} (u_{ik}^m)} \tag{5}$$

Finally, we compute the objective function related to Eq.(2) and check the criteria termination (the objective function convergence).

The fuzzy membership matrix U consist the degree of membership belonging to each cluster for every sample feature. We embed U, which has two degrees belonging to $T.gondii$ and host cell for each feature denoted as $U = \{U_{\mathcal{S}}, U_{\mathcal{T}}\}$, into our Cycle GAN, and design the fuzzy Cycle GAN loss for generators $\{G, F\}$ and discriminators $\{D_{\mathcal{S}}, D_{\mathcal{T}}\}$.

$$\begin{cases} L_F = \mathbb{E}_{x_{\mathcal{T}} \sim p_{data(\mathcal{T})}}[\log(U_{\mathcal{S}} - D_{\mathcal{S}}(F(x_{\mathcal{T}})))], \\ L_{D_{\mathcal{S}}} = \mathbb{E}_{x_{\mathcal{S}} \sim p_{data(\mathcal{S})}}[\log D_{\mathcal{S}}(x_{\mathcal{S}})] \\ \qquad + \mathbb{E}_{x_{\mathcal{T}} \sim p_{data(\mathcal{T})}}[\log(U_{\mathcal{T}} - D_{\mathcal{S}}(F(x_{\mathcal{T}})))], \end{cases} \tag{6}$$

$$\begin{cases} L_G = \mathbb{E}_{x_{\mathcal{S}} \sim p_{data(\mathcal{S})}}[\log(1 - D_{\mathcal{T}}(G(x_{\mathcal{S}})))], \\ L_{D_{\mathcal{T}}} = \mathbb{E}_{x_{\mathcal{T}} \sim p_{data(\mathcal{T})}}[\log D_{\mathcal{T}}(x_{\mathcal{T}})], \end{cases} \tag{7}$$

where $U_{\mathcal{S}}$ is the degrees of membership belonging to the shared cluster point of source banana images in $\mathcal{S}$ and $T.gondii$ images in $\mathcal{T}$, and $U_{\mathcal{T}}$ is the degrees of membership belonging to host cell cluster point in $\mathcal{T}$.

At the meanwhile, we design a target pulling loss on cluster points $V = \{v_{\mathcal{S}}, v_{\mathcal{T}}\}$ in target domains to pull the $T.gondii$ cluster point away from host cell with a larger distance. The function is followed:

$$L_{pulling} = -\|v_{\mathcal{S}}(C(F(x_{\mathcal{T}}))) - v_{\mathcal{T}}(C(F(x_{\mathcal{T}})))\|^2 \tag{8}$$

Algorithm 1 summarizes the main step of this sequential iterative algorithm with back-propagation and Lagrange Multiplier.

3 Network Architecture and Details

3.1 Architecture

The architecture of our method is composed by original Cycle GAN and VGG layers. Cycle GAN originally designs generators with multiple residual blocks [He *et al.*, 2016], and discriminators with several convolutional layers combined with binary L2 loss [Zhu *et al.*, 2017], which setting is followed to maintain the generative ability in CycleGAN. Differently, in our discriminators, we make several critical modifications with justifications.

First, using Vgg network [Simonyan and Zisserman, 2014] to learn feature representation is critical to maintain the discriminative information for microscopic images, as it has achieves much faster convergence and locally smooth results in malaria recognition [Rosado *et al.*, 2016]. Second, we adopt the degrees of membership of each sample into the generative adversarial loss function to enhance the generating ability of sample group belong the closed cluster between source domain, weaken the generating ability of sample group belong the distant cluster between source domain for generators and discriminators. Such approach can make the different group have a large distance between each of them.

3.2 Training Details

We implement our network on TensorFlow framework [Keeton and Roscoe, 2016] with Tesla K40C and 128G memory in Ubuntu 16.04 system, and use the Adam solver [Kingma and Ba, 2014] for FCGAN network with a learning rate of $2e$-4 and closely follow the settings of Cycle GAN and Vgg Network to train generators, discriminators and feature extractors. After jointly training for 4000 epoches, we apply early stop when the fuzzy loss no longer decreases for about 5 epochs (usually takes 4000 jointly training epochs to reach a desired point). In training, the number of training data in two domains can be different. Our parameterss in algorithm 1 are set as $m = 2$, $P = 2$ and $loop = 100$.

4 Experiments

4.1 Datasets and Experiment Settings

$Toxoplasma\ gondii$ microscopic images are captured under two brightfield light microscopies (Leica DM2700P and Olympus IX53), where preserved slices of parasites infection samples are mounted onto slides and stained with Giemsa. The first dataset is captured with 40X objectives (the magnification is 400X, T400) in Leica DM2700P microscope, and obtained original 8,156 $T.gondii$ images and 4,979 host cell images. The Second dataset is captured with 100X oil immersion objectives (the magnification is 1000X, T1000) in Olympus IX53 microscope, which obtains 6969 $T.gondii$ images and 8023 host cell images. In addition, we crawl 2382 banana images, and 2142 cat images on the internet as different source data, as the compared macroscopic associated object.

To overcome negative effects of variations in Figure 1, we adopt white balancing techniques to compensate some of these variations. For all images, we use white balancing technique pools the pixels from all fields of view and compute a global color balance affine transform for each image. In addition, we choose all images both in $\mathcal{S}$ and $\mathcal{T}$, then resize them in 256×256.

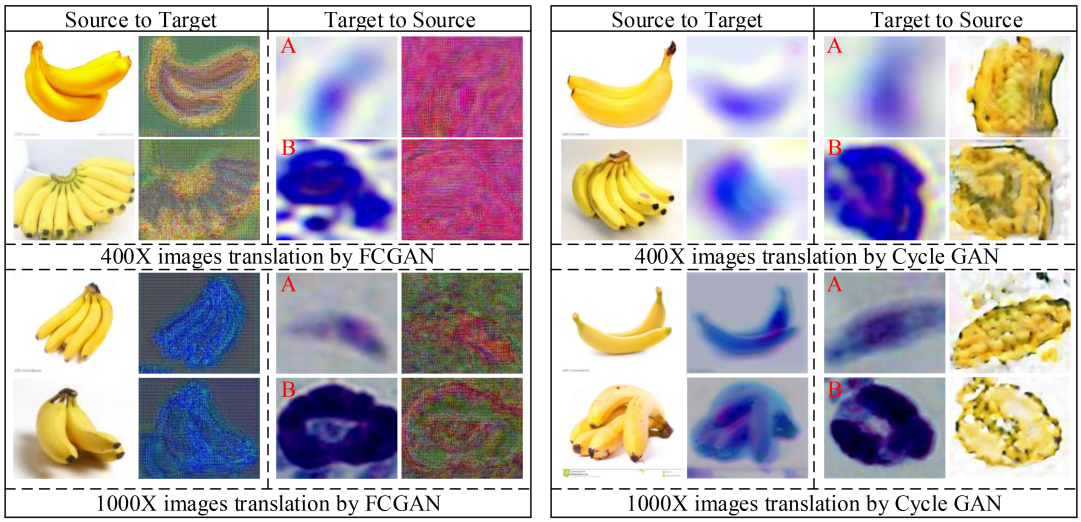

Figure 3: Image translation between source and target images in FCGAN and Cycle GAN. The red marker A in images denotes $T.gondii$ parasite and B denotes host cell.

Method	Accuracy	F1-score	Recall	Precision
ResNet	52.4%	0.688	0.996	0.525
VggNet	99.6%	0.994	0.993	0.996
GoogleNet	98.2%	0.983	0.971	0.996
VggFCM	52.3%	0.776	0.776	0.769
ResFCM	76.4%	0.79	0.791	0.879
GoogleFCM	48.6%	0.477	0.388	0.620
CycleFCM	97.2%	0.900	0.978	0.833
Ours+Cat	94.4%	0.952	0.912	0.996
Ours+Ban	**98.6%**	**0.988**	**0.986**	**0.991**

Table 1: Results of baselines and FCGAN on T400 dataset.

Method	Accuracy	F1-score	Recall	Precision
ResNet	47.8%	0.989	0.984	0.995
VggNet	90.8%	0.641	0.475	0.984
GoogleNet	61.7%	0.470	0.451	0.490
VggFCM	81.3%	0.823	0.923	0.743
ResFCM	53.5%	0.618	0.650	0.589
GoogleFCM	46.5%	0.431	0.401	0.466
CycleFCM	86.7%	0.837	0.774	0.912
Ours+Cat	83.6%	0.804	0.726	0.901
Ours+Ban	**88.3%**	**0.868**	**0.818**	**0.925**

Table 2: Result of baselines and FCGAN on T1000 dataset.

4.2 Baselines

To validate the effectiveness of our FCGAN approach on $T.gondii$ recognition task, we first compare FCGAN with three supervised deep CNN networks, including ResNet [He *et al.*, 2016], VggNet[Simonyan and Zisserman, 2014], GoogleNet [Szegedy *et al.*, 2017]. Besides, to discuss effects of components in our FCGAN, we implement some unsupervised extensive experiments to evaluate effects of each components in FCGAN. VggFCM (ResFCM, GoogleFCM) is a combination of VGG (Res, Google) network with fuzzy C-means cluster algorithm, and CycleFCM is combined the VGG+FCM and conventional Cycle GAN, which can prove the efficiency of the embedded fuzzy component in Cycle GAN. Furthermore, we choose cat as another source macroscopic object besides banana, because cat is not similar to $T.gondii$. That will prove the more similar source object, the better performance will be produced. These baselines are drawn in Table 1 and 2, where FCGAN with banana source is denoted as **Ours+Ban** and FCGAN with Cat source is denoted as Ours+Cat.

4.3 Results

Recognition Performance. The results in Table 1 and 2 illustrate recognition performance over 400X $T.gondii$ dataset and 1000X $T.gondii$ dataset for FCGAN and baselines. Our FCGAN with banana source data achieves the best performance in unsupervised models and it surpass two supervised deep learning model (ResNet and GoogleNet) with a only difference of 1% between VggNet. FCGAN with Banana source achieves a competitive results of 98.6% accuracy, 0.494 F1-score, 0.986 recall, and 0.991 precision on T400 dataset, and 88.3% accuracy, 0.434 F1-score, 0.818 recall, and 0.925 precision on T1000 dataset. It can be shown that our Micro-Macro associated object pulling strategy can achieve competitive results for unsupervised $Toxoplasma\ gondii$ recognition.

Comparison with supervised methods. To evaluate the competitiveness of our FCGAN, we select three widely used supervised CNN networks including VggNet, GoogleNet, and ResNet. As shown in Tables 1, it can be seen that ResNet, GoogleNet and VggNet obtain 55.4%, 98.2% and 99.6% accuracy in T400 dataset. Obviously, FCGAN+Banana model achieves the best result in all unsupervised methods, with

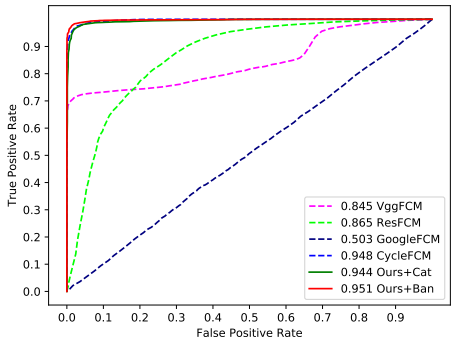

Figure 4: ROC curves for Toxoplasma recognition in different methods on T400 dataset. The AUC value is marked before the name of each method.

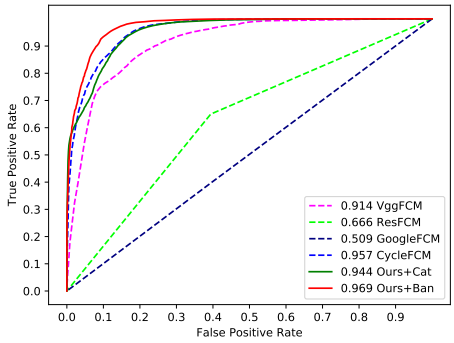

Figure 5: ROC curves for Toxoplasma recognition in different methods on T1000 dataset. The AUC value is marked before the name of each method.

98.6% accuracy, 0.494 F1-score, 0.986 Recall, and 0.991 Precision. The values of accuracy, F1-score, recall exceed both ResNet and GoogleNet, but close to VggNet. The precision surpass the ResNet, and close to VggNet and GoogleNet with a difference of 0.005. The results on T1000 dataset are similar. All those results demonstrate our FCGAN can achieve similar performance compared with supervised deep learning methods, while FCGAN do not require labeling any microscopic images. It should be emphasized that labeling $Toxosplasma\ gondii$ under microscope is highly time-consuming, labor intensive and needs well trained professionals to recognize.

Comparison with unsupervised methods. For comparison, we test four unsupervised baselines together with our FCGAN, including VggFCM, ResFCM, GoogleFCM and CycleFCM. The results are illustrated in Table 1 and 2, and Receiver Operating Characteristic (ROC) curves with AUC (area under the curve) value are drawn in Figure 4 and 5. As shown, it is easy to prove that our FCGAN achieves the best performance in unsupervised methods, leaving the baselines at least 1.4%(98.6%-97.2%) accuracy, 0.015 (0.434-0.419) F1-score, 0.008 (0.986-0.978) recall, and 0.013(0.925-0.912) precision on T400 dataset. The ROC curves in Figures 4 and 5 also demonstrate that our FCGAN draws a better curves than the unsupervised baselines with higher AUC value, leaving them at least 0.003 (0.951-0.948).

4.4 Disscusion

Evaluation of different macroscopic objects. To discuss the effectiveness of source object, we collect banana and cat images as source to conduct experiments. In morphology, cat is less similar to $T.gondii$ than banana, and its results and ROC curves have a distance between FCGAN+Banana in Table 1 and Figure 4. The same conclusion can be obtain in Table 2 and Figure 5. It can be seen that FCGAN+banana obtains a better performance than FCGAN+cat. That indicate the more similar of the macroscopic object, the better performance will be achieved in our FCGAN model.

Evaluation of Fuzzy component. In figure 3, we illustrate a few samples of the translated images $G(\mathcal{S})$ and $F(\mathcal{T})$. It can be observed that FCGAN makes translated images remaining shape and texture information, and following the same background of the domain from where they generated. But Cycle GAN make source and target images only follow mutual style translation, which can not alleviate the effect of variations in Figure 1. That is, our FCGAN can create the texture and shape relationship between microscopic object and macroscopic object with selectivity of associated information. The comparison of ours+Ban and cycleFCM can show that our FCGAN can achieve better performance, indicating FCGAN can exploit associated information (for example, shape and texture information) to boost the cluster results.

5 Conclusion

This paper is the first to study $Toxoplasma\ gondii$ recognition task and propose an unsupervised Fuzzy Cycle Generative Adversarial Network with transfer learning strategy. The model is inspired by the knowledge from parasitologist that $Toxoplasma\ gondii$ is in banana shaped form. Through the experiments on two $T.gondii$ microscopic image datasets with magnification of 400X and 1000X, we successfully demonstrate that our FCGAN model has stronger associated information selectivity and better pulling effect than other conventional models. Our method for Toxoplasma microscopic image analysis can potentially speed up the detection and pave the way for a rapid, low-cost diagnostics.

References

[Bezdek, 1973] James Christian Bezdek. Fuzzy mathematics in pattern classification. *Ph. D. Dissertation, Applied Mathematics, Cornell University*, 1973.

[Burrells *et al.*, 2018] Alison Burrells, Alessandra Taroda, Marieke Opsteegh, Gereon Schares, Julio Benavides, Cecile Dam-Deisz, Paul M. Bartley, Francesca Chianini, Isabella Villena, and Joke Van Der Giessen. Detection and dissemination oftoxoplasma gondiiin experimentally infected calves, a single test does not tell the whole story:. *Parasites and Vectors*, 11(1):45, 2018.

[Christiansen *et al.*, 2018] Eric M. Christiansen, Samuel J. Yang, D. Michael Ando, Ashkan Javaherian, Gaia Skibinski, Scott Lipnick, Elliot Mount, Alison O'Neil, Kevan Shah, and Alicia K. Lee. In silico labeling: Predicting fluorescent labels in unlabeled images. *Cell*, 173(3):S0092867418303647, 2018.

[Gecer *et al.*, 2018] Baris Gecer, Selim Aksoy, Ezgi Mercan, Linda G. Shapiro, Donald L. Weaver, and Joann G. Elmore. Detection and classification of cancer in whole slide breast histopathology images using deep convolutional networks. *Pattern Recognition*, 84:345–356, 2018.

[He *et al.*, 2016] Kaiming He, Xiangyu Zhang, Shaoqing Ren, and Jian Sun. Deep residual learning for image recognition. In *2016 IEEE Conference on Computer Vision and Pattern Recognition, CVPR 2016, Las Vegas, NV, USA, June 27-30, 2016*, pages 770–778, 2016.

[Keeton and Roscoe, 2016] Kimberly Keeton and Timothy Roscoe, editors. *12th USENIX Symposium on Operating Systems Design and Implementation, OSDI 2016, Savannah, GA, USA, November 2-4, 2016*. USENIX Association, 2016.

[Khan and Grigg, 2017] Asis Khan and Michael E Grigg. Toxoplasma gondii: Laboratory maintenance and growth. *Current protocols in microbiology*, 44(1):20C–1, 2017.

[Kingma and Ba, 2014] Diederik P. Kingma and Jimmy Ba. Adam: A method for stochastic optimization. *CoRR*, abs/1412.6980, 2014.

[Klir and Yuan, 1995] George J Klir and Bo Yuan. Fuzzy sets and fuzzy logic: theory and applications. (1):283–287, 1995.

[Loddo *et al.*, 2018] Andrea Loddo, Cecilia Di Ruberto, and Michel Kocher. Recent advances of malaria parasites detection systems based on mathematical morphology. *Sensors*, 18(2):513, 2018.

[Mehanian *et al.*, 2018] Courosh Mehanian, Ben Wilson, Cary Champlin, Earl Long, Stephane Proux, Dionicia Gamboa, Peter Chiodini, Jane Carter, Mehul Dhorda, and David Isaboke. Computer-automated malaria diagnosis and quantitation using convolutional neural networks. In *IEEE International Conference on Computer Vision Workshop*, pages 116–125, 2018.

[Rajaraman *et al.*, 2018] Sivaramakrishnan Rajaraman, Sameer K. Antani, Mahdieh Poostchi, Kamolrat Silamut, Md. A. Hossain, Richard J. Maude, Stefan Jaeger, and George R. Thoma. Pretrained convolutional neural networks as feature extractors toward improved malaria parasite detection in thin blood smear images. *Peerj*, 6(1), 2018.

[Rosado *et al.*, 2016] Luís Rosado, José M. Correia Da Costa, Dirk Elias, and Jaime S. Cardoso. Automated detection of malaria parasites on thick blood smears via mobile devices. *Procedia Computer Science*, 90:138–144, 2016.

[Simonyan and Zisserman, 2014] Karen Simonyan and Andrew Zisserman. Very deep convolutional networks for large-scale image recognition. *CoRR*, abs/1409.1556, 2014.

[Szegedy *et al.*, 2017] Christian Szegedy, Sergey Ioffe, Vincent Vanhoucke, and Alexander A. Alemi. Inception-v4, inception-resnet and the impact of residual connections on learning. In *Proceedings of the Thirty-First AAAI Conference on Artificial Intelligence, February 4-9, 2017, San Francisco, California, USA.*, pages 4278–4284, 2017.

[Xing *et al.*, 2018] Fuyong Xing, Yuanpu Xie, Hai Su, Fujun Liu, and Lin Yang. Deep learning in microscopy image analysis: A survey. *IEEE Trans. Neural Netw. Learning Syst.*, 29(10):4550–4568, 2018.

[Zhu *et al.*, 2017] Jun-Yan Zhu, Taesung Park, Phillip Isola, and Alexei A. Efros. Unpaired image-to-image translation using cycle-consistent adversarial networks. In *IEEE International Conference on Computer Vision, ICCV 2017, Venice, Italy, October 22-29, 2017*, pages 2242–2251, 2017.